Title: STRUCTURAL AND MAGNETIC PROPERTIES OF NANOCRYSTALLINE $Bi_{1-x}La_xFeO_3$ ($0.0 \leq x \leq 0.4$) SYNTHESIZED BY A MECHANOCHEMICAL ROUTE

Authors: Adrián A. Cristóbal, Cinthia P. Ramos, M.Susana Conconi, Paula G. Bercoff, Pablo M. Botta

PII: S0025-5408(16)32402-3
DOI: http://dx.doi.org/doi:10.1016/j.materresbull.2017.07.035
Reference: MRB 9464

To appear in: *MRB*

Received date: 26-12-2016
Revised date: 29-5-2017
Accepted date: 24-7-2017

Please cite this article as: Adrián A.Cristóbal, Cinthia P.Ramos, M.Susana Conconi, Paula G.Bercoff, Pablo M.Botta, STRUCTURAL AND MAGNETIC PROPERTIES OF NANOCRYSTALLINE Bi1-xLaxFeO3 ($0.0 \leq x \leq 0.4$) SYNTHESIZED BY A MECHANOCHEMICAL ROUTE, Materials Research Bulletinhttp://dx.doi.org/10.1016/j.materresbull.2017.07.035

STRUCTURAL AND MAGNETIC PROPERTIES OF NANOCRYSTALLINE $Bi_{1-x}La_xFeO_3$ ($0.0 \leq x \leq 0.4$) SYNTHESIZED BY A MECHANOCHEMICAL ROUTE

Adrián A. Cristóbal[1], Cinthia P. Ramos[2], M. Susana Conconi[3], Paula G. Bercoff[4], Pablo M. Botta[1]

[(1)]*Instituto de Investigaciones en Ciencia y Tecnología de Materiales (INTEMA), UNMdP-CONICET. J. B. Justo 4302 (B7608FDQ) Mar del Plata, Argentina.*

[(2)]*Gerencia Investigación y Aplicaciones (GIyA), Centro Atómico Constituyentes (CAC)-Comisión Nacional de Energía Atómica (CNEA), CONICET. Av. Gral. Paz 1499 (1650), San Martín, Buenos Aires, Argentina.*

[(3)]*Centro de Tecnología de Recursos Minerales y Cerámica (CETMIC), Cno. Centenario y 506, CIC-CONICET (B1897ZCA) M.B. Gonnet, Buenos Aires, Argentina*

[(4)]*Facultad de Matemática, Astronomía, Física y Computación (FaMAF), Universidad Nacional de Córdoba. Instituto de Física Enrique Gaviola (IFEG), CONICET. Medina Allende s/n, Ciudad Universitaria, Córdoba, Argentina.*

Graphical Abstract

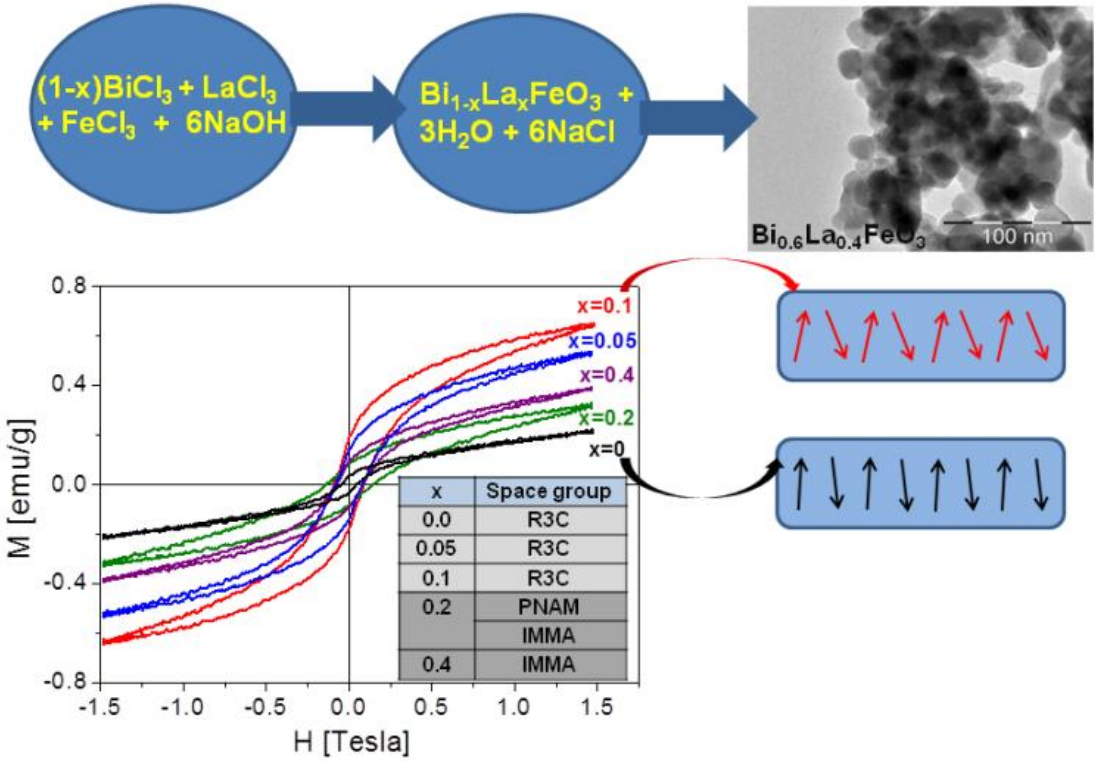

HIGHLIGHTS

- A mechanochemical reaction produces $Bi_{1-x}La_xFeO_3$ and NaCl in ambient conditions.
- Heating at 600ºC and ulterior washing yields ferrite phase for all the compositions.
- The synthesized powders consist of agglomerates of $Bi_{1-x}La_xFeO_3$ nanoparticles.
- La-content influences the crystal structure and Néel temperature of the materials.
- The presence of two canting levels of antiparallel spins causes a complex magnetism.

Abstract

$Bi_{1-x}La_xFeO_3$ ($0.0 \leq x \leq 0.4$) powders were prepared by means of a solid acid-base reaction induced by mechanochemical energy. Bi, La and Fe chlorides were high-energy ball-milled with NaOH, yielding a mixture of $Bi_{1-x}La_xFeO_3$ and NaCl. After heating and washing, nanoparticles of $Bi_{1-x}La_xFeO_3$ were obtained as a main product, with low contents of secondary phases. Structural characterization was performed by X-ray diffraction (Rietveld refinement) and Raman spectroscopy. The hyperfine magnetic behavior was analyzed by means of Mössbauer spectroscopy and the microstructure of the particles was evaluated by transmission electron microscopy. Differential scanning calorimetry was employed to investigate the thermal behavior of the samples and magnetic measurements at room temperature were also carried out. Crystal structure transitions as a function of composition were identified. Moreover, an intricate magnetic behavior was observed, which was explained on the basis of the concomitant contribution of two different canting levels of the antiparallel spins.

INTRODUCTION

Ferromagnetic and ferroelectric materials exhibit long-range ordering of magnetic or electric dipoles, which can be oriented by the application of a magnetic or electric external field, respectively. Magnetoelectric multiferroic materials simultaneously display ferroelectricity and ferromagnetism. This means that net magnetic moments can be induced by an external electric field, or electric polarization can be induced by a magnetic field [1-3]. Beside the academic interest drawn by this kind of solids, they become technologically attractive because both switching phenomena are the basis of non-volatile random access memory [4-5]. Magnetoelectric materials are promising candidates for low-power and high-density information storage, since they are able to combine fast electrical writing and magnetic reading [6].

The coexistence of both magnetic and electrical long-range orders at room temperature in a single crystalline structure is indeed a challenge for materials science. Conventional ferroelectricity requires solid lattices with closed-shell d^0 or s^2 cations; whereas for ferromagnetism, cations with d^n (or f^n) configurations and unpaired electrons are necessary. These opposite requirements leave only a few compounds with multiferroic properties [7].

One of the most widely investigated multiferroic compounds is $BiFeO_3$ (BFO). At room temperature, BFO adopts a rhombohedrally distorted perovskite structure (space group R3c). The pseudocubic (pc) unit cell has a lattice parameter - a_{rh} - of 3.965 Å and a rhombohedral angle - α_{rh} - between 89.3 and 89.4º, with ferroelectric polarization along the [111] direction. The unit cell can also be described in terms of hexagonal symmetry (hex), with the c-axis parallel to the diagonals of the perovskite cube ($[001]_{(hex)}$ //$[111]_{(pc)}$). Lattice parameters are a_{hex} = 5.58 Å and c_{hex} = 13.90 Å [8]. BFO has an intricate magnetic structure, where the local ordering is G-type antiferromagnetic with each Fe^{3+} ion surrounded by six antiparallel spins. In BFO, $6s^2$ lone-pair of Bi^{3+} ions located in A sites are the responsible for the ferroelectrical polarization along the $[111]_{pc}$ direction [9]. Weak magnetoelectric coupling leads to a slight canting of the magnetic moment that averages to zero due to a long range incommensurate spin cycloid, with a wavelength $\lambda \approx 62$ nm [10].

In spite of being a promising material, BFO presents several drawbacks, such as large coercive fields and high leakage currents, which can be detrimental for some applications [11]. In order to overcome these problems, the addition of different substituents in $BiFeO_3$, taking the positions of

either Bi or Fe, has been widely studied [12-14]. Transition, rare earth and alkaline earth metals have all been employed to improve the dielectric and magnetic properties of BFO.

On the other hand, obtaining pure BFO is not a simple task, because of the formation of secondary phases (mainly $Bi_{25}FeO_{39}$ and $Bi_2Fe_4O_9$), which lead to a degradation of the electrical and magnetic properties [15, 16]. Partial substitution of Bi^{3+} ions by lanthanides sometimes avoids the formation of these undesired phases during synthesis. One of the most studied systems is $Bi_{1-x}La_xFeO_3$. It has been reported that La substitution increases the ferromagnetic moment and significantly reduces leakage current [17]. However, there exists a debate about the nature of phase transitions as a function of La content. Values of x between 0.1 and 0.3 have been reported for the rhombohedral to orthorhombic transition [18-20]. Furthermore, the rhombohedral and other phases may coexist at the composition limits of each phase. One of the causes for this disagreement can be the influence of preparation conditions (starting materials, temperatures, annealing times, etc.) on the structural stability of $Bi_{1-x}La_xFeO_3$ [20].

As for most of perovskite oxides, the mainly used synthesis route for BFO is the classic solid-state reaction between oxides or other reactants. In the last years several chemical methods, such as sol-gel [21], hydrothermal [22], co-precipitation [23] and microemulsion [24], have been employed to prepare nanocrystalline pure and doped BFO [25]. Additionally, a few articles report the use of mechanochemistry to obtain BFO [26-29]. This method has been used for decades as a tool to enhance the reactivity of solids and synthesize a wide variety of materials, including special alloys, mixed oxides, organic compounds and composites [30, 31].

Briefly, mechanochemical synthesis consists of a high energy milling of solid reactants, introducing a significant concentration of defects in their crystal structures. This accelerates diffusive processes in solid phases, increasing their reactivity. Under very energetic milling conditions and/or by employing highly reactive precursors, chemical reactions between solids can be completed in the mill at room temperature (or close). If milder conditions and/or less reactive precursors are used, a decrease of the reaction temperature is often observed. The main advantages of the mechanochemical methods are the simplicity, the possibility of producing relatively large material amounts, the absence of organic solvents and the use of low heating temperatures. Recently, the synthesis of $Bi_{1-x}La_xFeO_3$ in a wide composition range from mechanochemical treatment of Bi, La and Fe oxides was reported [32]. Pure phases were obtained, but using a high pressure of oxygen (7 bar) during the milling process.

A particular set of acid-base solid reactions were developed under mechanochemical conditions with the aim of producing several single oxides (TiO_2, Fe_2O_3, ZnO, etc) [33, 34]. In this method, metallic salts are milled together with a base (alkaline hydroxides, oxides or carbonates) to produce a solid mixture of a nanocrystalline oxide and a soluble by-product, which can be easily removed by washing. A remarkable advantage, when compared to conventional mechanosynthesis, is the limited growing of the particle size of the product phase. As the milling time increases, the crystallite size of reactants decreases, reaching nanometric dimensions. This very small size accelerates the acid-base reaction, favoring its occurrence at room temperature. The product phase crystals reproduce the nanometric dimensions of the milled reactants, forming a solid mixture in which each oxide nanoparticle is surrounded by the soluble salt phase [34]. Although this route was employed to prepare several single oxides, there is little previous work dealing with mixed oxides [29, 35].

In this work we report the synthesis of nanocrystalline $Bi_{1-x}La_xFeO_3$ using a mechanochemical acid-base reaction. The interest in the chosen composition range ($0.0 \leq x \leq 0.4$) resides in focusing on the structural transitions and their influence on the magnetic properties of the so prepared materials.

EXPERIMENTAL

Starting materials were $BiCl_3$, $FeCl_3.6H_2O$, $LaCl_3.7H_2O$ and NaOH, all commercial reagents (purity higher than 99 %). Several mixtures with different stoichiometry were prepared according to the reaction:

$$(1\text{-}x)BiCl_3 + xLaCl_3 + FeCl_3 + 6NaOH \rightarrow Bi_{1-x}La_xFeO_3 + 3H_2O + 6NaCl \qquad (1)$$

where x was varied from 0.0 to 0.4.

The solid mixtures were high-energy milled in a Fritsch Pulverissette 7 planetary ball mill, using vials of 45 cm^3 and balls of 1.5 cm diameter, both made of WC. Each vial was charged with 4 balls and 5 g of powder, giving a mass ratio of 22. The vials were rotated at 1500 rpm during 9 h.

After milling, the samples were heated at 600ºC for 1h under air atmosphere. These powders were washed with distilled water, filtered and dried at 60ºC for several hours. This operation was

performed with the aim to eliminate the by-product NaCl formed during the reaction. This series of samples was named BLFO-x, being x the La content in each mixture.

Phase identification and crystal structure of the samples was determined by X-ray diffraction (XRD), using a PANalytical X'Pert Pro diffractometer with CuKα radiation (λ = 0.154 nm) and a graphite monochromator. Scans were performed with an acquisition time of 10 s per point, using a resolution of 0.02º 2θ. Fullprof software was used for Rietveld refinements. The sizes of coherently diffracting domains were calculated by line profile analysis, corrected for instrumental peak broadening, by using a highly crystalline quartz specimen as standard.

Particle size and morphology were analyzed by transmission electron microscopy (TEM). Images were obtained using a Philips CM 200 UT microscope equipped with an ultra-twin objective lens. The electron source used was a LaB_6 filament operated at 200 keV.

Mössbauer spectra were taken at room temperature (RT) with a conventional constant acceleration spectrometer in transmission geometry with a ^{57}Co/Rh source. The absorber thickness was chosen to be the optimum according to the Long et al. criterion [36]. Least-squares fitting of the spectra were performed by using the Normos program [37]. Isomer shift (IS) values are given relative to that of α-Fe at RT.

Raman spectroscopy was performed at RT using an Invia Reflex confocal Raman microprobe with an Ar ion laser of 514 nm wavelength and a 10 μm spot in backscattering mode. An exposure time of 20 s and 3 accumulations were used, with a 50X objective. The laser power was reduced to 10% to prevent damage by heating (0.2 mW).

Differential scanning calorimetry (DSC) was carried out in a Shimadzu DSC-50 calorimeter to study the thermal behavior of samples between RT and 450 ºC. A heating rate of 10 ºC min^{-1} and approximately 20 mg of sample were used.

Magnetization (M) at RT as a function of magnetic field (H) was measured using a Lakeshore 7300 vibrating sample magnetometer. Hysteresis loops between +15 and -15 kOe were recorded.

RESULTS AND DISCUSSION

XRD patterns for the whole series are displayed in Figure 1, where the main indexed phase is $Bi_{1-x}La_xFeO_3$. Some very low-intensity peaks corresponding to spurious phases, such as $Bi_2Fe_4O_9$, $Bi_{24}Fe_2O_{39}$ and $Bi_{25}FeO_{40}$ were detected in the x = 0.0 and 0.4 samples, but no evidence of these secondary phases was perceived for samples with x = 0.05, 0.1 and 0.2.

Rietveld refinement analyses showed that, when increasing La content, a shift of the diffraction peaks to higher angles with respect to the BFO peak positions is noticeable. This is in coincidence with the lattice contraction produced by the replacement of Bi^{3+} cations by the La^{3+} smaller ones. Lattice parameters and space groups for the whole series are shown in Table 1. A continuous decrease of unit cell volume with x can be observed, as also reported by Perejon et al. [32]. Moreover, changes in the space group take place throughout the studied compositional range. The space group is rhombohedral (R3c) for x values up to 0.1, in agreement with the structure of the parent compound (BFO). These results are in accordance with some of those reported for samples prepared by other methods [20, 32].

For x = 0.2 and 0.4, the crystalline system changes to orthorhombic. The indexing of sample BLFO-0.2 was tested in the Imma, Pnam and $Pn2_1a$ space groups. For Pnam and Imma space groups the refinement gave a similar goodness of fit; however, space group $Pn2_1a$ gave a larger weighted profile factor Rwp (17.0) than that obtained for Pnam (9.38) using the same profile, instrumental parameters and refining atomic coordinates. For this reason, Table 1 does not include the results obtained from space group $Pn2_1a$. The refinement results are not in complete agreement with those previously reported by other authors [20, 32]. Rusakov et al. [20] proposed a coexistence of two structures with space groups R3c and Pnam for $0.15 < x < 0.17$ and the presence of an incommensurately modulated phase (Imma) for $0.19 < x < 0.30$. They used much higher heating temperatures, being that a possible explanation for the observed discrepancy with our results. Moreover, lower synthesis temperatures produce materials with broad diffraction peaks, making difficult the identification of contributions belonging to very similar structures.

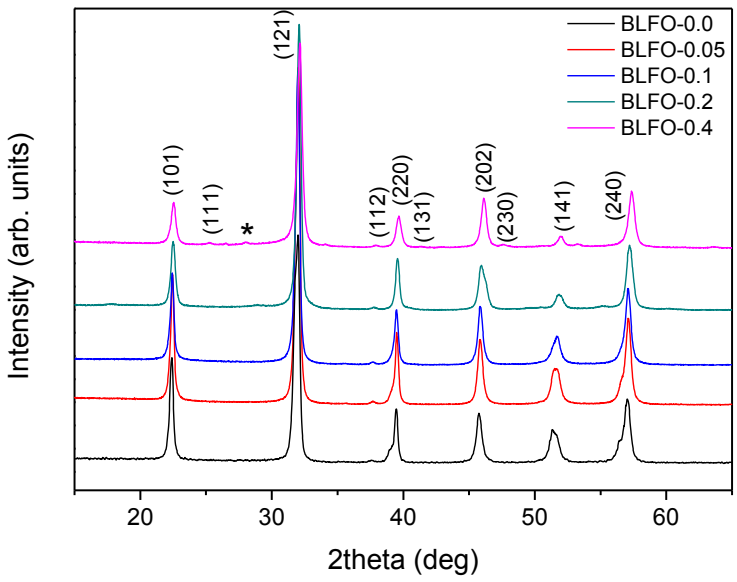

Figure 1. XRD patterns for the series BLFO-x. Peaks corresponding to perovskite $Bi_{1-x}La_xFeO_3$ are indexed. The small peak marked with * belongs to $Bi_{24}Fe_2O_{39}$ (some peaks corresponding to $Bi_2Fe_4O_9$ and $Bi_{25}FeO_{40}$ are too small to be marked).

The XRD peaks are broad due to the nanometric size of the crystallites and the microstrains induced by the milling. Crystallite sizes, determined using an isotropic model for peak broadening, decrease with La content, as shown in Table 1. These values have only a comparative meaning due to the use of an isotropic simplified model. This is also confirmed by TEM observations (Figure 2) where a smaller particle size, related to crystallite size, is evident from the x = 0.4 micrograph. A visual comparison reveals particle sizes between 25 and 50 nm for BLFO-0.1, whereas for BLFO-0.4 particle size is ranged between 10 and 20 nm. For all the samples, particles seem to be monocrystalline or formed by only a few nanometric crystallites, which in some cases show the presence of necks among them. This is a consequence of an incipient material transport that takes place during the thermal treatment. The resulting particles form aggregates with sizes ranging between 200 and 300 nm.

Table1. Structural parameters for the BLFO-x series. V: unit cell volume; Z: formula units per unit cell.

x	Space group	Lattice Parameters (Å)			V/Z $(Å)^3$	Crystallite size (nm)
		a	b	c		
0.0	R3C	5.5773 (2)	5.5773 (2)	13.8514(3)	62.19	74
0.05	R3C	5.5793 (3)	5.5793 (3)	13.8063 (5)	62.03	60
0.1	R3C	5.5785 (2)	5.5785 (2)	13.7525 (3)	61.77	66
0.2	PNAM	5.5990 (5)	11.2376 (7)	15.6893 (3)	61.70	62
	IMMA	5.6102 (6)	7.8514 (5)	5.5844 (6)	61.50	
0.4	IMMA	5.5993 (5)	7.8465 (5)	5.5572 (2)	61.04	25

x = 0.0

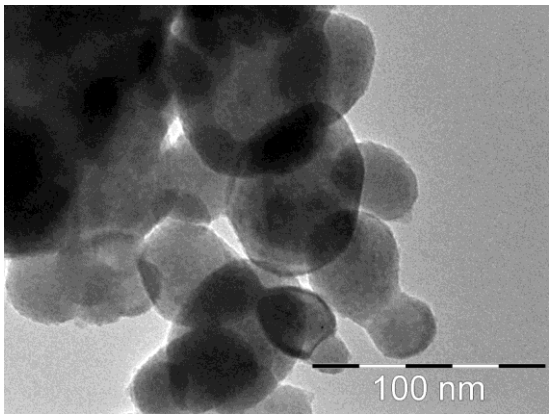

x = 0.05

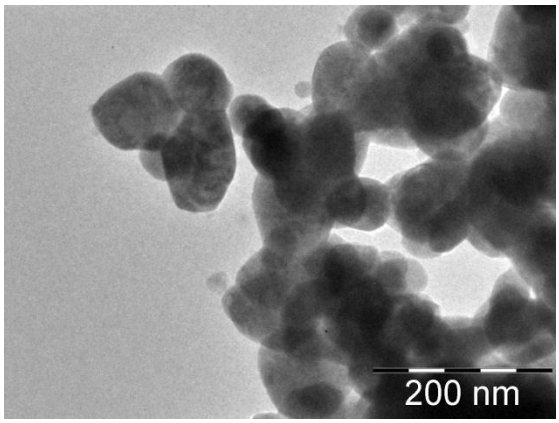

x = 0.1

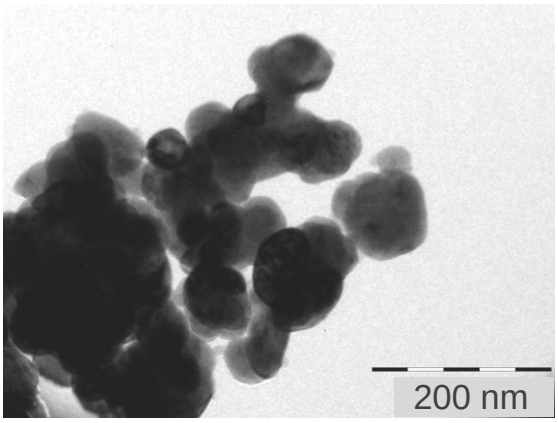

x = 0.2

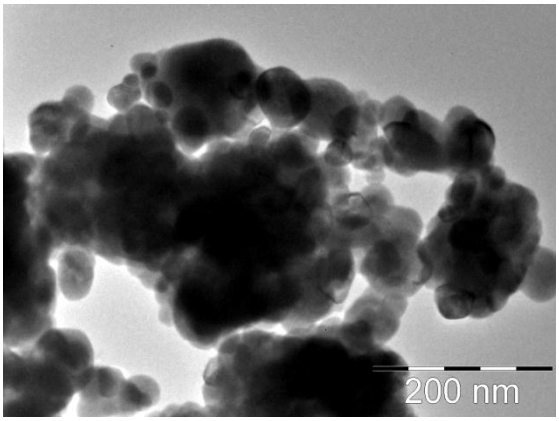

x = 0.4

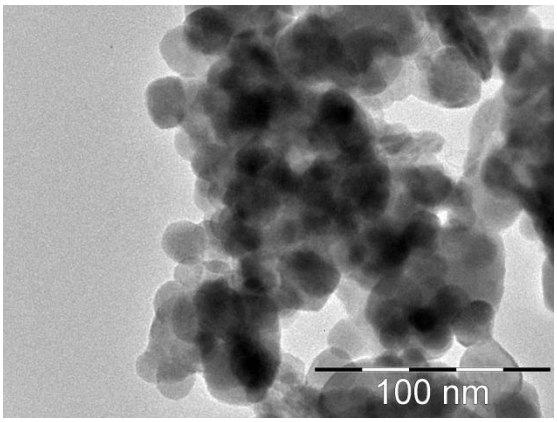

Figure 2. TEM micrographs for the whole series BLFO-x.

Figure 3 displays Raman spectra of the series BLFO-x in the 100-700 cm^{-1} range, where the first-order Raman active modes are noticeable. Each peak corresponds to a different vibrational mode of the $Bi_{1-x}La_xFeO_3$ structure. According to group theory, pure $BiFeO_3$ with rhombohedral structure has 13 Raman-active modes: $4A_1+9E$, while pure $LaFeO_3$ with orthorhombic structure has 21 Raman-active modes: $7A_g + 2B_{1g} + 7B_{2g} + 5B_{3g}$ [38].

Three strong peaks at 137, 166, and 217 cm^{-1} and nine weak peaks at 258, 360, 473, 525, 608, 677, 853, 1094, and 1280 cm^{-1} can be seen in spectra belonging to rhombohedral structures (x = 0.0, 0.05 and 0.1), which are consistent with previous works [39-42].

For samples BLFO-0.2 and BLFO-0.4 the most **noticeable** feature is the marked decrease of the intensities of the modes below 200 cm^{-1} and the disappearance of that at around 250 cm^{-1}. Such a phenomenon suggests that the lattice structure for these two compositions undergoes significant changes. Low frequency modes can be interpreted as external modes due to the relative motion of A-site cations in the oxygen octahedrons. The intensity of the A_1 modes below 250 cm^{-1} is reduced due to the decrease in the percentage of the Bi–O bond with large La substitution [38]. Another interesting characteristic is the appearance of two modes (visualized as one band) at around 400 cm^{-1}, which enhance gradually for larger x. These modes belong to the fingerprint peaks of the orthorhombic $LaFeO_3$ [43], indicating that the orthorhombic structure begins to emerge when the La content increases to 0.2.

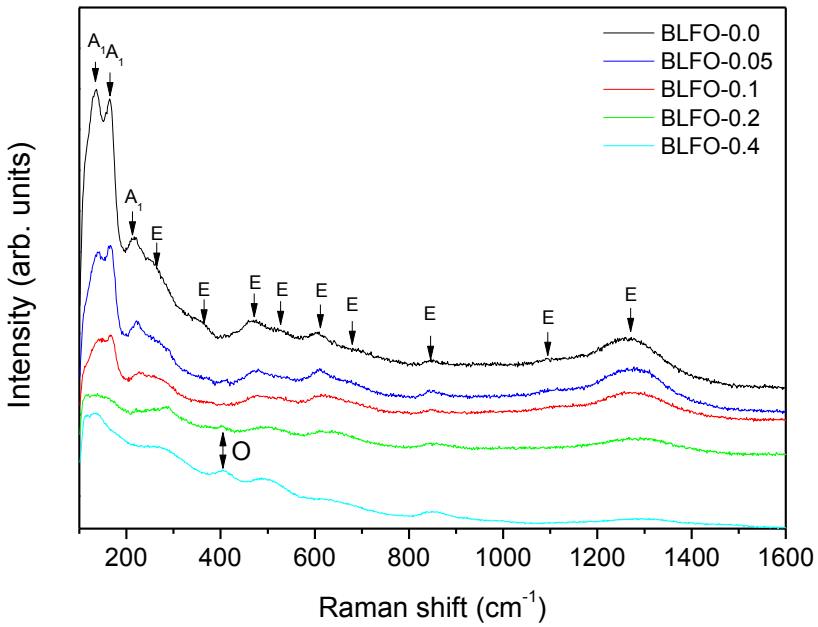

Figure 3. Raman spectra for the series BLFO-x. Vibrational modes (A_1 and E) corresponding to R3c structure are marked. The characteristic band for orthorhombic phase is indicated with O.

In Figure 4a, DSC measurements from RT to 450 ºC for BLFO-x samples on the whole range of compositions ($0.0 \leq x \leq 0.4$) are displayed. A change in the position of the curve slope approximately from 372 ºC for x = 0.0 to 396 °C for x = 0.4 can be observed, which is attributed to the Néel (antiferromagnetic-paramagnetic) transition [32, 44]. For x = 0.0, the obtained Néel temperature (T_N) is in good agreement with the reported values [44]. A consistent increase of T_N with x is observed (Figure 4b), which is an expected behavior considering that for $LaFeO_3$, T_N = 465 ºC [45].

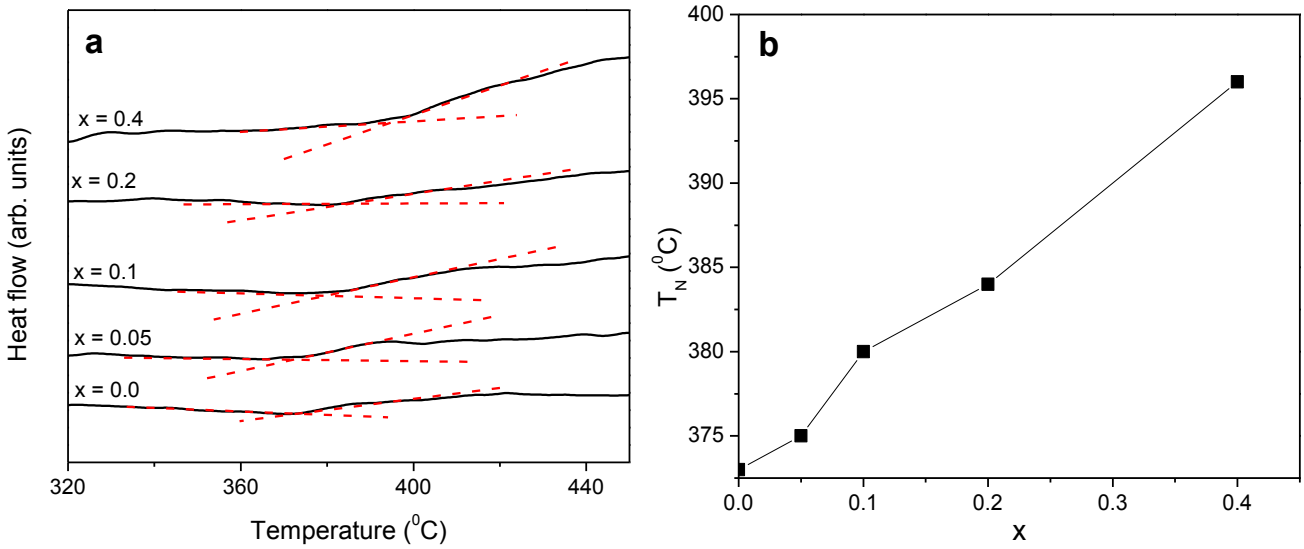

Figure 4. DSC measurements (a) and Neél temperature (b) for the series BLFO-x.

The spin cycloid structure of bulk BFO, with a characteristic wavelength of about 62 nm, does not allow the appearance of net magnetization. However, magnetization can be enhanced due to surface induced magnetism in small particles (< 62 nm) [46]. The ball milling process performed in this work produced BFO nanoparticles smaller than 100 nm, as shown by TEM images.

It is known that rare-earth substitution in perovskites can improve the magnetic properties of these materials [47, 48]. There are some factors that are important in order to evaluate changes in magnetization after Bi^{3+} substitution by rare-earth cations in nanoparticulate systems. These factors are related to changes in the structure when the cation is incorporated into the perovskite lattice, with the magnetic nature of the dopant ions (in this case La^{3+} is a non-magnetic ion) and with a possible variation in oxygen stoichiometry -that is, a Fe^{2+} contribution. For elucidating this last issue, Mössbauer spectroscopy is a very useful technique.

Mössbauer spectra of the series BLFO-x (Figure 5) were fitted considering two major sextets (S1 and S2), a minor sextet (S3) and two doublets (D1 and D2). Even when Bi has a very high absorption coefficient for 14.4 keV Mössbauer gamma rays, resulting in spectra with less

statistics -although taken during long measuring times-, the spectra are clear enough to distinguish every component.

Sextets S1 and S2 indicate a magnetically ordered state with values typical of high spin Fe^{3+} and are attributed to the nanostructured $Bi_{1-x}La_xFeO_3$ oxide. The corresponding hyperfine parameters for these two sextets are listed in Table 2. From Figure 5 it is clear that, for undoped and lightly doped samples (BLFO-0.0 and BLFO-0.05), the spectra are asymmetric due to an appreciable contribution of the spiral rotation of magnetic moments in these samples. However, the spectra become more symmetric on increasing doping, as a consequence of the suppression of spiral spin structure in highly doped samples [49].

The paramagnetic doublets (D1 and D2) are attributed to the secondary phases $Bi_2Fe_4O_9$ and $Bi_{25}FeO_{40}$ [50] which may be segregated on account of an incomplete reaction between the precursors. The non-magnetic nature of this impurity phases should not affect the magnetic properties of the samples. Due to a broad distribution of particle size in the samples, a little contribution of some small nanoparticles (< 20 nm) with superparamagnetic behavior is not discarded. The low fractions of these phases are similar for all the samples, amounting less than 4 % of the iron phases in every case. It is important to remark that Mössbauer spectroscopy is more sensitive than XRD to detect these secondary phases.

For the minor sextet (S3, with Bhf ~ 46 T)), the isomer shift (IS) and quadrupole shift (2ε) values point out to a high-symmetry cubic spinel (IS ~ 0.6 mm/s, 2ε ~ 0 mm/s). This sextet suggests the presence of non-equivalent octahedral sites in Fe_3O_4. In the first instance, the presence of Fe_3O_4 was not noticed by XRD, but considering the possibility of a very small fraction of this phase distinguished by Mössbauer spectroscopy, a very slow scan (20 s per step) around the highest intensity peak of magnetite at 35.4° 2θ was performed (Figure 6). A little contribution of this phase was confirmed in all the samples, except for BLFO-0.4, supporting Mössbauer results. This fact should be taken into account for subsequent analysis of the magnetic properties because magnetite could contribute to magnetization.

The major sextets (S1 and S2) in the spectrum of sample BLFO-0.0 account for two different sites displaying different 2ε values, which are assigned to different trigonal distortions of the octahedral environment. The zero value for 2ε in S2 suggests a symmetrical octahedral site

meanwhile that in S1 points out to a lower symmetry site. This change is due to the variation in the angles between the principal axis of the electric field gradient (EFG) and the spin direction. In this sense, the distortion in the S1 site implies a Dzyaloshinskii-Moriya (DM) interaction with a consequent net magnetization, responsible for the small hysteresis seen in the M-H loop (see Figure 7). These facts let us associate the S2 site with an antiferromagnetic (AF) state and the S1 site with a weakly ferromagnetic (WF) state. The difference between the two kinds of contributions is also reflected in the hyperfine field values (B_{hf}), being B_{hf} (S1) > B_{hf} (S2) (see Table 2).

Doping with La still yields two subspectra corresponding to different surroundings of the Fe atoms. With La addition up to x = 0.1, there is an increment of the S1 area fraction denoting a stronger canting of spins (Table 2) and accordingly, the net magnetization increases (Table 3 and Figure 7). For x = 0.2, this fraction slightly decreases, likely as a result of the crystalline structure change already demonstrated by XRD and Raman analyses; then a consequent reduction of net magnetization is expected. This was confirmed by magnetization measurements (Table 3 and Figure 7). Finally, for x = 0.4, Mössbauer results are very similar to those of x = 0.2, but there is a slight increase in magnetization (Table 3 and Figure 7), probably because of the total suppression of the spin cycloid structure produced by the small particle size in this sample (~ 25 nm), which is under the characteristic wavelength [10]. The change in group structure seen by XRD should also be considered to explain this effect.

The IS values for S1 and S2 in the La-doped samples are typical of Fe^{3+} in octahedral sites. No signature of different valence of Fe is observed; then the possibility of oxygen vacancies is discarded as a modifying factor in magnetization. These IS values suffer no variation with successive La incorporation, indicating the same s-electron density at the Fe nucleus in both kind of sites.

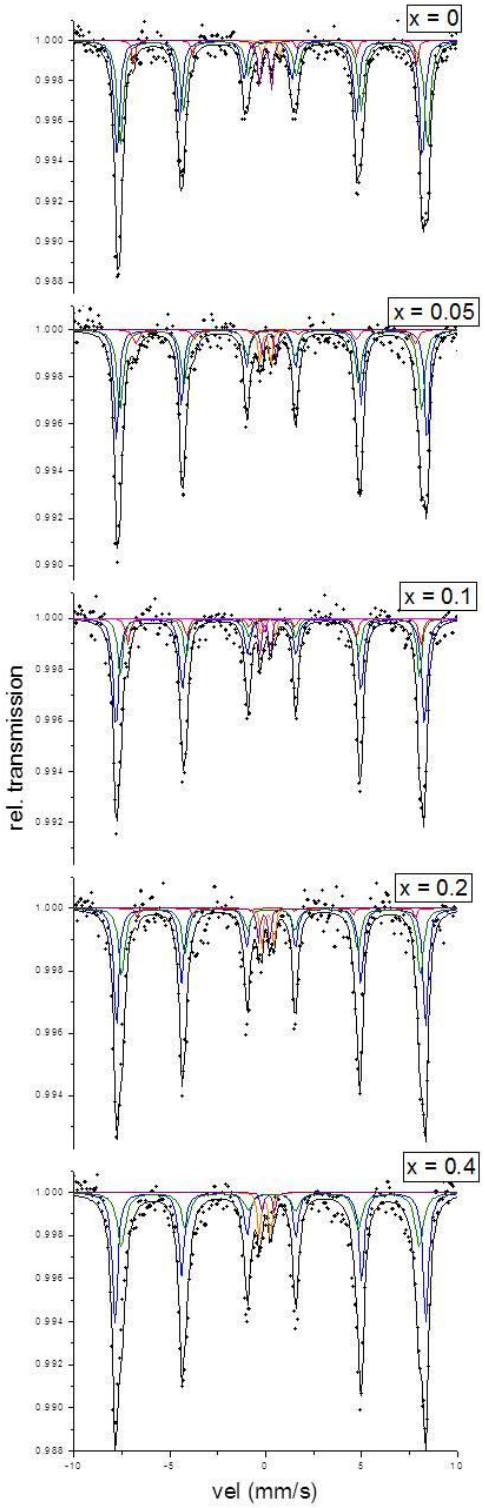

Figure 5. Fitted Mössbauer spectra for samples BLFO-x.

Table 2. Hyperfine parameters and relative area ratios for the different sites in samples BLFO-x.

x	Subspectra	IS [mm/s]	2ε [mm/s]	B_{hf} [T]	Relative area ratio (S1/S2)
0.0	S1	0.35	0.25	50.3	0.33
	S2	0.40	0.00	49.1	
0.05	S1	0.41	0.03	50.2	0.78
	S2	0.39	-0.02	48.8	
0.1	S1	0.39	-0.08	49.9	2.15
	S2	0.39	-0.14	48.4	
0.2	S1	0.39	-0.06	50.1	1.09
	S2	0.40	-0.01	48.3	
0.4	S1	0.39	-0.06	50.3	1.04
	S2	0.40	-0.09	48.2	

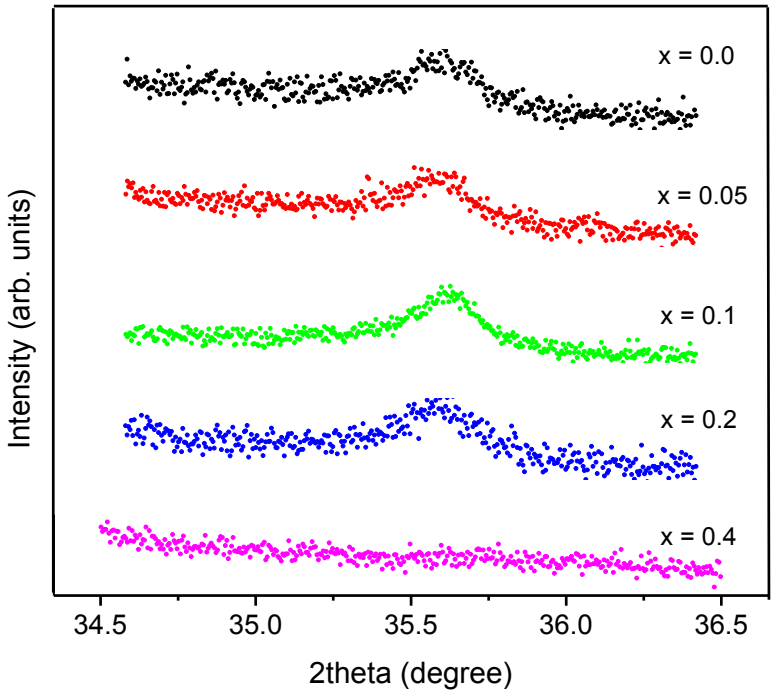

Figure 6. XRD slow scan around the high-intensity peak of magnetite (3 1 1).

RT magnetization measurements (M vs H) for samples BLFO-x are shown in Figure 7. The magnetic hysteresis observed for BLFO-0.0 confirms a WF contribution in addition to the typical AF nature of BFO. A significant increment in magnetization for samples with x= 0.05 and 0.1 and a later decrease for the x = 0.2 and 0.4 samples, are in agreement with Mössbauer results.

VSM is an appropriate characterization technique for determining the macroscopic magnetic variables. The actual nature of the spin ordering can only be determined by means of other techniques. Therefore, a canted AF magnetic ordering will be noticed as a ferromagnetic (FM) contribution in the hysteresis loop. All the measured M vs H curves of Figure 7 were fitted with two FM contributions (FM1 and FM2), with the usual function used to represent a FM hysteresis curve [51]:

$$M(H) = \frac{2Ms}{\pi}\tan^{-1}\left[\frac{H \pm Hc}{Hc}\tan\frac{\pi}{2}\frac{Mr}{Ms}\right],$$

where Mr and Ms are the remanent and saturation magnetizations, respectively, and Hc is the coercive field. Figure 8 shows the fit for sample BLFO-0.1, which is representative of all the set.

The values of Ms and Hc for each contribution, as well as the r^2 (figure of merit) of the fits are given in Table 3.

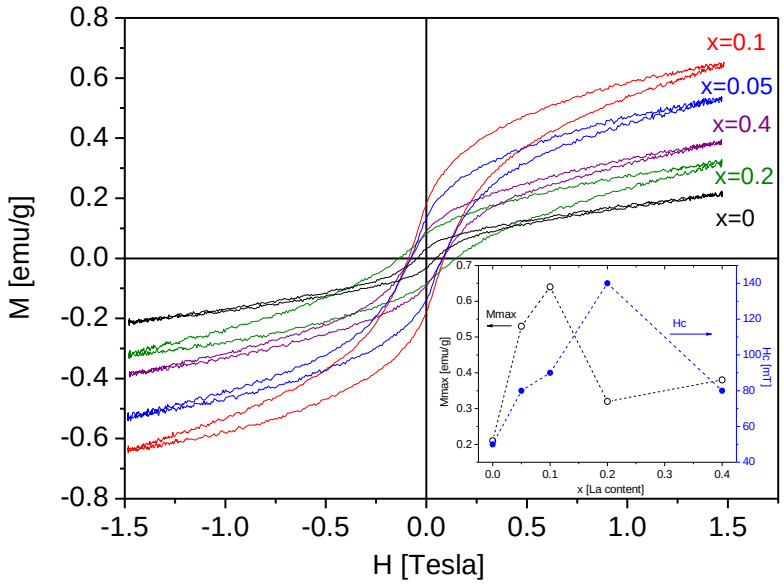

Figure 7. Room temperature hysteresis loops for the BLFO-x series. The inset shows maximum magnetization Mmax (left axis) and coercivity Hc (right axis) as a function of La content, x.

Table 3. Maximum magnetization (Mmax) and coercive field (Hc) obtained from the measured hysteresis loops shown in Figure 7. Saturation magnetization (Ms), remanent magnetization (Mr) and coercive field (Hc) of the two FM contributions (1 and 2) used for the fitting of the M vs H curves and figure of merit of the fit (r^2).

x	Mmax [emu/g]	Hc [mT]	FM1			FM2			r^2
			Ms1 [emu/g]	Mr1 [emu/g]	Hc1 [mT]	Ms2 [emu/g]	Mr2 [emu/g]	Hc2 [mT]	
0.0	0.21	50	0.34	0.01	40.8	0.07	0.03	45.6	0.9965
0.05	0.53	80	0.49	0.01	44.8	0.28	0.12	75.6	0.9986
0.1	0.64	90	0.47	0.01	43.3	0.38	0.17	85.6	0.9994
0.2	0.32	140	0.40	0.01	63.7	0.14	0.07	125.8	0.9981
0.4	0.38	80	0.48	0.03	58.4	0.17	0.06	77.4	0.9987

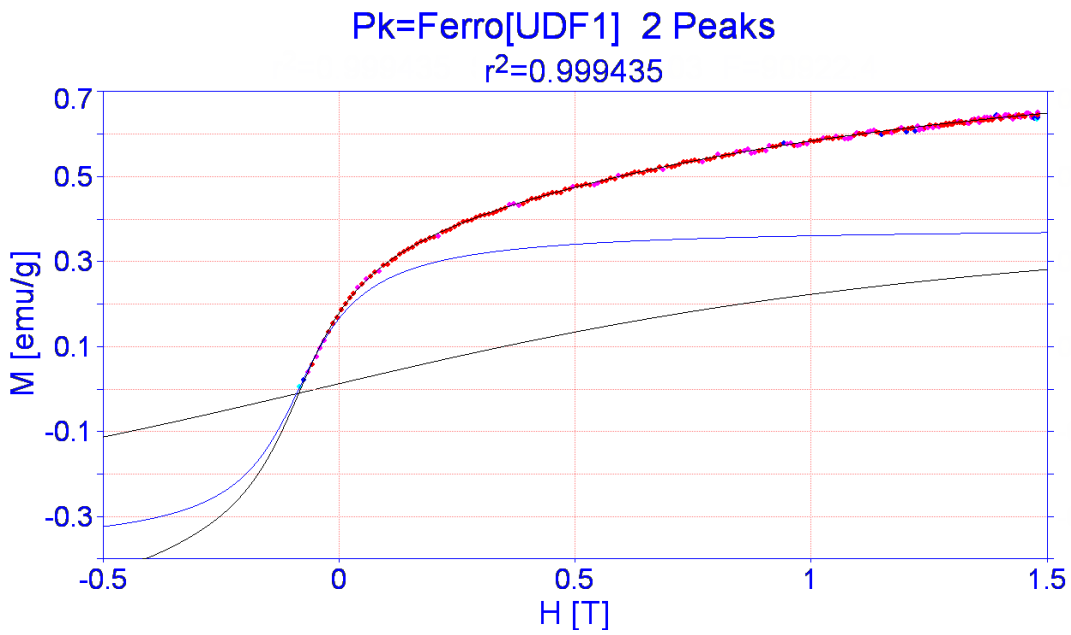

Figure 8: Fit of the upper branch of the M vs H curve corresponding to sample BLFO-0.1, using two FM contributions.

According to the values of Mr and Hc obtained in the fits, it is possible to assign FM1 and FM2 contributions to analogue sites detected by Mössbauer spectroscopy (S1 and S2), denoting a stronger canting of spins for the FM1 (S1 sites in Table 2) contribution. It is evident that none of the samples exhibit saturation magnetization, as a consequence of the presence of antiferromagnetic coupling; however, the slopes of the curves at high magnetic fields are not the same, indicating different amounts of FM1 and FM2 contributions in each sample, as it was determined by Mössbauer spectroscopy.

The high Hc value for BLFO-0.2 may be caused by the higher magnetocrystalline anisotropy of the orthorhombic structure as compared to the samples with lower La content. This result may hint the coexistence of the Pnam and Imma structures in this sample.

CONCLUSIONS

Nanocrystalline $Bi_{1-x}La_xFeO_3$ ($0 \leq x \leq 0.4$) was synthesized by a mechanochemical acid-base reaction, followed by a thermal treatment at 600ºC and washing. As a result, pure materials, with very low contents of secondary phases, were obtained. The microstructure of the powders consisted of agglomerates of nanoparticles with sizes between 10 and 50 nm.

XRD Rietveld refinements and Raman spectroscopy allowed to identify a structural transition from a rhombohedral (R3c) to an orthorhombic (Pnam or Imma) lattice at $0.10 < x < 0.20$. For higher La contents the structure crystallized in an Imma space group.

Mössbauer spectroscopy analysis ruled out the presence of Fe^{2+}. The increasing spin canting with La incorporation up to $x = 0.1$ enhanced the net magnetization. A little contribution from magnetite as an impurity cannot be discarded. For $x = 0.2$, a decrease in magnetization was observed mainly as a result of a structural transition. For $x = 0.4$, on account of the breaking of the spin cycloid modulation, a small increase in magnetization is observed; maybe due to the uncompensated surface spins induced by the reduction in grain size. A change in the crystal structure of this sample might also contribute to this effect.

Based on our results, mechanosynthesized $Bi_{1-x}La_xFeO_3$ with $x \sim 0.1$ seems to be a propitious material for multiferroic devices. Even more, the variation in both the crystalline and magnetic structures with subtle changes in the perovskite composition makes this material easily tunable for different applications.

ACNOWLEDGEMENTS

The authors gratefully thank CONICET, UNMdP and ANPCyT for the financial support given to this work.

REFERENCES

[1] W. Eerenstein, N.D. Mathur, J.F. Scott, Multiferroic and magnetoelectric materials, Nature. 442 (2006) 759–765.

[2] N.A. Spaldin, M. Fiebig, Current trends of the magnetoelectric effect, Eur. Phys. J. B. 71 (2009) 293–297.

[3] C.A.F. Vaz, J. Hoffman, C.H. Ahn, R. Ramesh, Magnetoelectric coupling effects in multiferroic complex oxide composite structures, Adv. Mater. 22 (2010) 2900-2918.

[4] M. Bibes, and A. Barthélémy, Multiferroics: towards a magnetoelectric memory. Nat. Mater. 7 (2008) 425–426.

[5] J. Ma, J. Hu, Z. Li, C.W. Nan, Recent progress in multiferroic magnetoelectric composites: from bulk to thin films, Adv. Mater. 23 (2011) 1062-1087.

[6] J. F. Scott, Data storage: multiferroic memories. Nature Mater. 6 (2007) 256–257.

[7] N. A. Hill, Why are there so few magnetic ferroelectrics? J. Phys. Chem. B. 104, (2000) 6694–6709.

[8] G. Catalan, J.F. Scott, Physics and applications of bismuth ferrite, Adv. Mater. 21 (2009) 2463-2485.

[9] C. Ederer, N. A. Spaldin, Weak ferromagnetism and magnetoelectric coupling in bismuth ferrite, Phys Rev B. 71 (2005) 60401-60404.

[10] D. Lebeugle, D. Colson, A. Forget, M. Viret, A. M. Bataille, A. Gukasov, Electric-field-induced spin flop in $BiFeO_3$ single crystals at room temperature, Phys. Rev. Lett., 100 (2008) 227602 (1-4).

[11] B. Xu, D. Wang , J. Íñiguez, L. Bellaiche, Finite Temperature Properties of Rare-Earth-Substituted $BiFeO_3$ Multiferroic Solid Solutions, Adv. Funct. Mater. 25 (2014) 552-558.

[12] C. Yang, D. Kan, I. Takeuchi, V. Nagarajan, J. Seidel, Doping $BiFeO_3$: approaches and enhanced functionality, Phys. Chem. Chem. Phys. 14 (2012) 15953–15962.

[13] A.K. Ghosh, G.D. Dwivedi, B. Chatterjee, B. Rana, A. Barman, S. Chatterjee, H.D. Yang, Role of codoping on multiferroic properties at room temperature in $BiFeO_3$ ceramic, Solid State Comm. 166 (2013) 22-26.

[14] M.R. Suchomel, C.I. Thomas, M. Allix, M.J. Rosseinsky, A.M. Fogg, High pressure bulk synthesis and characterization of the predicted multiferroic $Bi(Fe_{1/2}Cr_{1/2})O_3$, Appl. Phys. Lett. 90 (2007) 112909 (1-3).

[15] A. Reetu, S. Agarwal, A. Sanghi, Rietveld analysis, dielectric and magnetic properties of Sr and Ti codoped $BiFeO_3$ multiferroic, J. Appl. Phys. 110 (2011) 073909 (1-6).

[16] S.M. Selbach, M.A. Einarsrud, T. Grande, On the thermodynamic stability of $BiFeO_3$, Chem. Mater. 21 (2008) 169-173.

[17] L.H. Yin, B.C. Zhao, J. Fang, R.R. Zhang, X.W. Tang, W.H. Song, J.M. Dai, Y.P. Sun, Improved leakage current and ferromagnetic properties in magnetic field annealed $BiFeO_3$-based ceramics, J. Solid State Chem. 194 (2012) 194–198.

[18] D. Kothari, S. Upadhy, C. Meneghini, V.R. Reddy, G. Aquilanti, A. Gupta, Structural and magnetic study of La doped multiferroic $BiFeO_3$, Solid State Phys. 1447 (2012) 1319–1320.

[19] Q.R. Yao, J. Cai, H.Y. Zhou, G.H. Rao, Z.M. Wang, J.Q. Deng, Influence of La-doping on structure and magnetic behaviors in $BiFeO_3$, J. Alloy. Compd. 633 (2015) 170–173.

[20] D.A. Rusakov, A. M. Abakumov, K. Yamaura, A. A. Belik, G. Van Tendeloo, E. Takayama-Muromachi, Novel self-crosslinked poly (aryl ether sulfone) for high alkaline stable and fuel resistant alkaline anion exchange membranes, Chem. Mater. 23 (2011) 285–292.

[21] Q.R. Yao, Y.H. Shen, P.C. Yang, H.Y. Zhou, G.H. Rao, Z.M. Wang, J.Q. Deng, Structure, phase diagram and magnetic properties of $Bi_{1-x}La_xFeO_3$ solid solution Ceram. International. 42 (2016) 6100–6106.

[22] X. Yan, J. Chen, Y. Qi, J. Cheng, Z. Meng, Hydrothermal synthesis and characterization of multiferroic $Bi_{1-x}La_xFeO_3$ crystallites J. Eur. Ceram. Soc. 30 (2010) 265–269.

[23] H. Ke, W.Wang, Y. Wang, J. Xu, D. Jia, Z. Lu, Y. Zhou, Factors controlling pure-phase multiferroic $BiFeO_3$ powders synthesized by chemical co-precipitation, J. Alloy. Compd. 509 (2011) 2192-2197.

[24] N. Das, R. Majumdar, A. Sen, H.S. Maiti, Mater Lett. 61(2007) 2100-2104.

[25] Q. Zhang, D. Sando and V. Nagarajan, Chemical route derived bismuth ferrite thin films and nanomaterials, J. Mater. Chem. C. 4 (2016) 4092-4124.

[26] I. Szafraniak, M. Po1omska, B. Hilczer, A. Pietraszko, L. Kepinski, Characterization of $BiFeO_3$ nanopowder obtained by mechanochemical synthesis, J. Eur. Ceram. Soc. 27 (2007) 4399-4402.

[27] D. Maurya, H. Thota, K. S. Nalwa, and A. Garg, $BiFeO_3$ ceramics synthesized by mechanical activation assisted versus conventional solid-state-reaction process: A comparative study, J. Alloy. Compd. 477 (2009) 780–784.

[28] A. Perejón, N. Maso, A.R. West, P.E. Sanchez-Jimenez, R. Poyato, J. M. Criado, and L.A. Perez-Maqueda, Electrical properties of stoichiometric $BiFeO_3$ prepared by mechanosynthesis with either conventional or spark plasma sintering, J. Am. Ceram. Soc. 96 (2013)1220–1227.

[29] A.A. Cristóbal, P.M. Botta, Mechanochemically assisted synthesis of nanocrystalline $BiFeO_3$, Mater. Chem. Phys. 139 (2013) 931-935.

[30]. S.L. James, C.J. Adams, C. Bolm, D. Braga, P. Collier, T. Frisci , Mechanochemistry: opportunities for new and cleaner synthesis, Chem. Soc. Rev. 41 (2012) 413-447.

[31] V. Sěpelák, A. Düvel, M. Wilkening, K-D. Becker and P. Heitjans, Mechanochemical reactions and syntheses of oxides, Chem. Soc. Rev. 42 (2013) 7507-7520.

[32] A. Perejón, P.E. Sanchez-Jimenez, L.A. Perez-Maqueda, J.M. Criado, J. Romero de Paz, R. Saez-Puche, N. Maso and A.R. West, Single phase, electrically insulating, multiferroic La-substituted $BiFeO_3$ prepared by mechanosynthesis, J. Mater. Chem. C, 2 (2014) 8398-8411.

[33] P.G. McCormick, T. Tsuzuki, J.S. Robinson, J. Ding, Nanopowders synthesized by mechanochemical processing, Adv. Mater. 13 (2001) 1008-1010.

[34] T. Tsuzuki, P.G. McCormick, Mechanochemical synthesis of nanoparticles, J. Mater. Sci. 39 (2004) 5143-5146.

[35] M. Muroi, P.G. McCormick, R. Street, Surface spin disorder and exchange bias in $La_{0.7}Ca_{0.3}MnO_3$ nanoparticles synthesised by mechanochemical processing, Rev. Adv. Mater. Sci 5 (2003) 76-81.

[36] G.J. Long, T.E. Cranshaw, G. Longworth, The ideal Mössbauer effect absorber thickness, Mössbauer Effect Reference and Data Journal 6 (1983) 42-49.

[37] R. A. Brand, Normos program, Internat. Rep. Angewandte Physik , Univ. Duisburg, 1987.

[38] Y. Yang, Y. Liu, K. Zhu, L. Zhang., S. Ma, J. Liu, Y. Jiang, Structural properties of $Bi_{1-x}La_xFeO_3$ studied by micro-Raman scattering, Chin. Phys. B 19 (2010) 37802 (1-6).

[39] G. L. Yuan, S. W. Or and L. W. Chan, Structural transformation and ferroelectric–paraelectric phase transition in $Bi_{1-x}La_xFeO_3$ (x = 0 – 0.25) multiferroic ceramics
J. Phys. D. 40 (2007) 1196-1200.

[40] M. K. Singh, H. M. Jang, S. Ryu and M. H. Jo, Polarized Raman scattering of multiferroic $BiFeO_3$ epitaxial films with rhombohedral R3c symmetry, Appl.Phys. Lett. 88 (2006) 42907 (1-3).

[41] M. K. Singh, S. Ryu and H. M. Jang, Polarized Raman scattering of multiferroic $BiFeO_3$ thin films with pseudo-tetragonal symmetry, Phys. Rev. B 72 (2005) 132101 (1-4).

[42] Y. Yang, J. Y. Sun, K. Zhu, Y. L. Liu and L .Wan, Structure properties of $BiFeO_3$ films studied by micro-Raman scattering, J. Appl. Phys. 103 (2008) 093532 (1-6).

[43] J. Andreasson, J. Holmlund, R. Rauer, M. Käll, L. Börjesson, C.S. Knee, A.K. Eriksson, S-G. Eriksson, M. Rübhausen, and R.P. Chaudhury, Electron-phonon interactions in perovskites containing Fe and Cr studied by Raman scattering using oxygen-isotope and cation substitution, Phys. Rev. B 78 (2008) (1-13).

[44] G.A. Smolenski, V.M. Yudin, E.S. Sher, Y.E. Stolypin, Antiferromagnetic properties of some perovskites, Sov. Phys. JETP 16 (1963) 622–624.

[45] D. Treves, Studies on orthoferrites at the Weizmann Institute of Science, J. Appl. Phys. 36 (1965) 1033–1039.

[46] T. Park, G. C. Papaefthymiou, A. J. Viescas, A. R. Moodenbaugh and S. S. Wong, Size-Dependent Magnetic Properties of Single-Crystalline Multiferroic $BiFeO_3$ Nanoparticles, Nano Lett. 7 (2007) 766-772.

[47] F. Z. Qian, J. S. Jiang, S. Z. Guo, D. M. Jiang and W. G. Zhang, Multiferroic properties of $Bi_{1-x}Dy_xFeO_3$ nanoparticles,J. Appl. Phys. 106 (2009) 84312 (1-6).

[48] R. K. Mishra, D. K. Pradhan, R. N. P. A. Choudhary Banerjee, Effect of yttrium on improvement of dielectric properties and magnetic switching behavior in $BiFeO_3$, J. Phys. Condensed Matter 20 (2008) 45218 (1-6).

[49] D. Lebeugle, D. Colson, A. Forget, M. Viret, P. Bonville, J. F. Marucco, and S. Fusil, Room-temperature coexistence of large electric polarization and magnetic order in $BiFeO_3$ single crystals, Phys. Rev. B 76 (2007) 24116 (1-27).

[50] M. Ncube, D. Naidoo, K. Bharuth-Ram, D. Billing, H. Masenda, D. R. Sahu, B. K. Roul, R. M. Erasmus, XRD and Mössbauer spectroscopy study of Ho doped $BiFeO_3$, Hyperfine Interact. 219 (2013) 83–88.

[51] M. Stearns, Y. Cheng, Determination of para and ferromagnetic components of magnetization and magnetoresistance of granular Co/Ag films, J. Appl. Phys. 75 (1994) 6894-6899.